Magnetization reversal process and magnetic relaxation of self-assembled Fe_3Pt nanowire arrays with different diameters: Experiment and micromagnetic simulations

Jian-Hua Gao, Da-Li Sun, Qing-Feng Zhan, Wei He, and Zhao-Hua Cheng*
State Key Laboratory of Magnetism and Beijing National Laboratory for Condensed Matter Physics, Institute of Physics, Chinese Academy of Sciences, Beijing 100080, China

(Received 7 September 2006; revised manuscript received 27 November 2006; published 23 February 2007)

Magnetization reversal process and magnetic relaxation of Fe_3Pt nanowire arrays fabricated by electrodeposition have been investigated by means of micromagnetic simulation and magnetization measurements. Time dependence of magnetization reveals that the nanowire arrays exhibit a strong magnetic viscosity effect. The magnetic viscosity coefficients S, which are dependent on temperature and magnetic field, achieve maximum values near the coercivity. The activation volume V^*, defined as the effective volume involved in the magnetization reversal process, increases with temperature as $T^{1/2}$ and linearly with the diameter, which is consistent with the theoretical prediction of the thermally activated magnetization reversal process.

DOI: 10.1103/PhysRevB.75.064421 PACS number(s): 75.60.Jk, 75.60.Lr, 75.75.+a

I. INTRODUCTION

Magnetic properties of magnetic nanowire arrays have been extensively investigated because of their potential applications in ultrahigh-density magnetic recording media as well as their significance in fundamental research. Owing to the strong magnetic shape anisotropy,[1,2] magnetic nanowire arrays exhibit both high coercive fields and squareness ratio with the easy magnetization direction along the wire axes. The fundamental issues include the shape anisotropy, the dipolar interaction between the nanowires, and size effect on magnetic properties.[3–5] Among them, the understanding of the magnetization reversal process for magnetic nanowires is of primary importance, and consequently, the emphasis has been put on the magnetization reversal mechanism and related magnetic behavior.[6–10] Several experimental techniques, such as micro-superconducting quantum interference device (SQUID) magnetometry,[11–14] ferromagnetic resonance,[15,16] and magnetic force microscopy[17] have been employed to investigate the magnetization reversal process of nanoparticles and nanowires. The results showed that the magnetization reversal of particles could be described by the classical Néel-Brown model for rotation in unison. However, as far as the magnetic wires are concerned, the magnetization reversal appears to proceed with inhomogeneous reversal mode, such as curling or nucleation followed by the propagation of the domain wall.

It is well known that the thermal stability is very critical to the high-density magnetic recording media with areal density of $Tbits/in^2$. Therefore, in addition to the static magnetic properties, the potential application of the nanowire arrays also depends on the hysteresis properties and dynamical behavior concerning the thermally activated magnetization reversal process and magnetic relaxation. Although such experiments have been performed on bulk materials and magnetic thin films,[18–20] the detailed magnetic viscosity behavior for nanowire arrays has rarely been reported.

In our previous work, shape anisotropy and temperature dependence on the magnetic properties with thermally activated reversal mechanism of the Fe_3Pt nanowire arrays have been investigated.[21] In this work, we simulated the magnetization reversal process of a hexagonal cell of 4×4 array for Fe_3Pt nanowires with $d=10$ nm. The simulated coercivity is in good agreement with the experimental one. Furthermore, time dependence of magnetization indicates that the nanowire arrays exhibit a strong magnetic viscosity effect, which was discussed in terms of the Stoner-Wohlfarth model.

II. EXPERIMENT

The Fe_3Pt nanowire arrays were fabricated by ac deposition into the anodic aluminum oxide (AAO) templates with different diameters. The AAO templates were prepared by a two-step anodization process controlled by the anodization voltage and electrolyte such as sulfuric acid and oxalic acid. Transmission electron microscopy (TEM) indicates that the nanowire diameters vary from about 8 to 60 nm. Fe_3Pt nanowires were electrodeposited into self-assembled nanoporous templates by ac deposition in the electrolytes consisted of 45 g/l HBO_3, 0.03M $FeSO_4$, and 0.01M $Pt(NO_2)_2(NH_3)_2$ with the pH value of 3.0–3.3. The ac deposition process was conducted under 15 V_{ac} with the frequency of 200 Hz for 300 s. The structural characterization of the Fe_3Pt nanowire arrays was performed using x-ray diffraction pattern and TEM, which indicate that the Fe_3Pt nanowires have fcc structure with the [110] preferred orientation along the nanowire axes.

The magnetic properties of the Fe_3Pt nanowire arrays have been investigated by means of SQUID magnetometry with the applied field parallel and perpendicular to the nanowire axes, respectively. It was revealed that the shape magnetic anisotropy plays a dominant role in the overall magnetic anisotropy of the nanowire arrays, driving the easy magnetization axis along the wire axes. The temperature dependence of coercivity has been interpreted by the thermally activated magnetization reversal process with the Stoner-Wohlfarth model. In order to understand the magnetization reversal process at ground state, micromagnetic simulation with the three-dimensional version of the OOMMF code was performed to simulate the hysteresis loop of the Fe_3Pt nanowire arrays.[22] In addition, we have investigated the magnetic relaxation of the Fe_3Pt nanowire arrays.

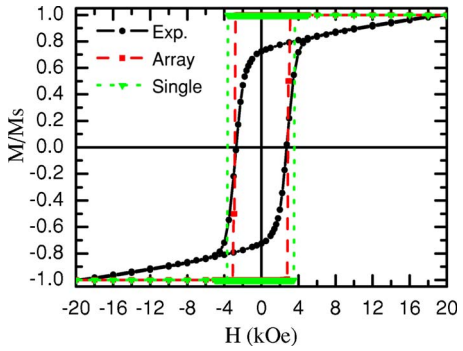

FIG. 1. (Color online) Measured (closed circles) and simulated (solid squares) hysteresis loops with the field applied parallel to the wire axis for Fe_3Pt nanowire arrays. The green line with triangles is the hysteresis loop for one single Fe_3Pt nanowire for comparison.

III. RESULTS AND DISCUSSIONS

Figure 1 illustrates the easy axis hysteresis loop for Fe_3Pt nanowire arrays with diameter of 10 nm measured by SQUID magnetometer at $T=5$ K. Although the shape magnetic anisotropy plays a dominant role in the overall magnetic anisotropy of the nanowire arrays of Fe_3Pt nanowire arrays, the coercivity parallel to the nanowires of 2.72 kOe is much smaller than the shape anisotropy field of 7.8 kOe. The large discrepancy between measured coercivity and shape anisotropy field implies that the exchange coupling of nanoparticles in one nanowire and the magnetostatic interaction between nanowires cannot be neglected. Modeling an array with macroscopic dimensions to compare with experimental value is difficult due to the large number of wires. Previous simulation of magnetostatically coupled Ni nanowires demonstrated that the coercivity decreases with increasing number of interacting wires and the simulated coercivity approaches to the experimental value when the numbers of interacting wires increase up to 16.[23] In order to take into account the interaction with neighboring wires and, at the same time, use reasonable computational time, the following model and parameters were assumed on the basis of our experimental results.

(1) A hexagonal cell of 4×4 array of Fe_3Pt nanowires was chosen to simulate the magnetization reversal process. The nanowire diameter $d=10$ nm, wire length $L=400$ nm, the center-to-center spacing between the wires is 40 nm, and the unit cell size is $1.25\times1.25\times10$ nm^3.

(2) Although it is well known that the magnetic properties change significantly in nanostructure, the saturation magnetization and exchange stiffness are very close to those of corresponding bulk materials in nanowire arrays when the diameter is up to 10 nm. Therefore, it is reasonable to use approximately the saturation magnetization of $M_S=1250$ emu/cm^3 and the exchange stiffness of $A=2.57\times10^{-12}$ A/m for the bulk $Fe_{75}Pt_{25}$.[24]

(3) Fe_3Pt is known as soft magnetic with easy magnetization axes along the [100] direction, and the nanowire arrays fabricated by electrodeposition are disordered fcc structures with [110] preferred direction along the nanowire axis. The Fe_3Pt nanowire arrays exhibit strong uniaxial magnetic anisotropy due to the shape anisotropy, which is much higher than magnetocrystalline anisotropy. From the magnetic hysteresis loops it could be seen that the switching field is much higher than the magnetocrystalline anisotropy field, which is usually several hundreds of oersteds. Although its magnetocrystalline anisotropy constant is not known, the fcc structure with high symmetry for Fe_3Pt suggests its magnetocrystalline anisotropy constant is the same order of magnitude as that for Fe. Previous investigation for Fe nanowire arrays indicated that the shape anisotropy constant is 1 order of magnitude larger than that of the magnetocrystalline anisotropy constant K_1.[21,25] Hence, the magnetocrystalline anisotropy can be neglected reasonably.

The simulated hysteresis loop for the Fe_3Pt nanowire arrays is plotted in Fig. 1. For comparison, the hysteresis loop for one single Fe_3Pt nanowire was also simulated and plotted in Fig. 1. The coercivity decreases from 3.7 kOe for one single nanowire to 2.8 kOe for 4×4 array of Fe_3Pt nanowires. The simulated value of coercivity is in good agreement with the measured coercivity $H_{C\|}$. However, the remanence squareness $S_\|$ exists with a relatively large deviation, which is related to the surface magnetic moment of the magnetic moments deviating from the wire axes of the nanowires.

The magnetization configuration of the Fe_3Pt nanowire arrays near the coercivity can give insight into the magnetization reversal. Since the nucleation starts at the end of the wire and the rest of the sample remains mostly homogeneously magnetized, we only plot the magnetization state in the region of 40 nm from the bottom of Fe_3Pt nanowire arrays [Fig. 2(a)] and a full view of magnetization configuration for one central nanowire [Fig. 2(b)]. An applied field of −3.0 kOe results in most of the magnetic moments for nanowires being switched in the direction of the applied field ($-z$ direction). Note that this field is not strong enough to switch a single decoupled wire (3.7 kOe). The reversal of some wires occurs because the stray field of neighboring wires adds to the external field and leads to a higher field to switch the magnetic moment. From the magnified view on the top of one nanowire [Fig. 2(c)], it can be seen that the magnetic moments start to rotate out from the easy axis at the ends of the nanowires, implying that the nucleation mode for the nanowires with $d=10$ nm deviates slightly from homogeneous rotation.

The magnetization reversal and coercivity of the nanowires are very sensitive to the nanowire diameter. Shtrikman and co-workers have predicted that for perfect infinite cylinders with different diameters, the magnetization reversal occurs by coherent rotation, magnetization curling, and buckling mode.[26,27] Usually coherent or uniform rotation occurs when the nanowire diameters are smaller than the critical diameter $d_{coh}=\sqrt{24A/\mu_0 M_S^2}$.[28] When the diameters are larger than the critical diameter d_{coh}, the magnetization reversal process occurs by magnetization curling mode or buckling mode.

For the magnetization curling mechanism, coercive fields decrease with increasing diameter and could be written as

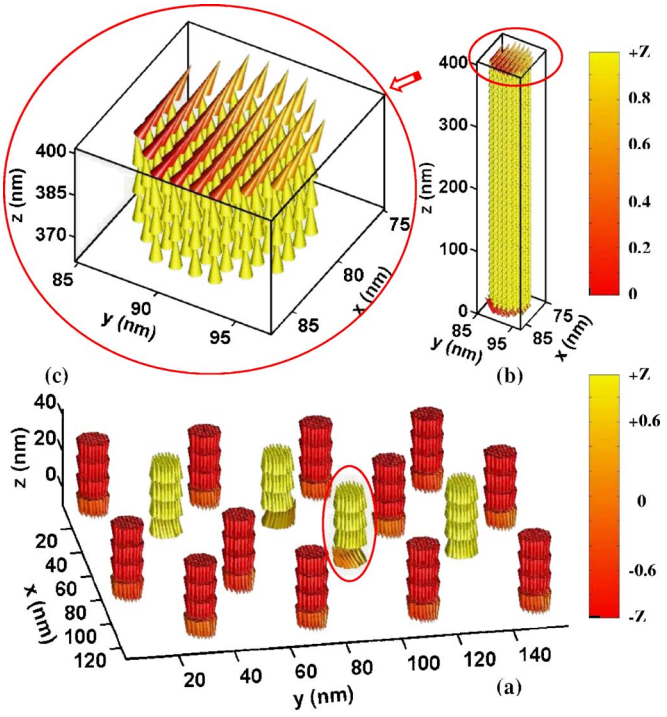

FIG. 2. (Color online) (a) Magnetization state at the bottom of a hexagonal cell of 4×4 arrays for Fe_3Pt nanowires with $d=10$ nm in the magnetic field of $H=-3.0$ kOe. (b) Magnetization configuration of one central nanowire. (c) Magnified view on the top of one nanowire. The colors represent the z component of the magnetization. The yellow (light gray) cones are magnetized states, whereas the red (dark gray) cones represent the states of magnetization that have switched for (a) and the remanent state for (b) and (c), respectively.

$$H_{c\|}=\frac{2\pi kA}{\mu_0 M_s}\frac{1}{d^2}+H_a, \tag{1}$$

where A is the exchange stiffness, k is the geometry dependent parameter, and d is the diameter of the nanowires. Figure 3 plots the coercivity parallel to the nanowire axes as a function of nanowire diameter at 5 and 300 K, respectively.

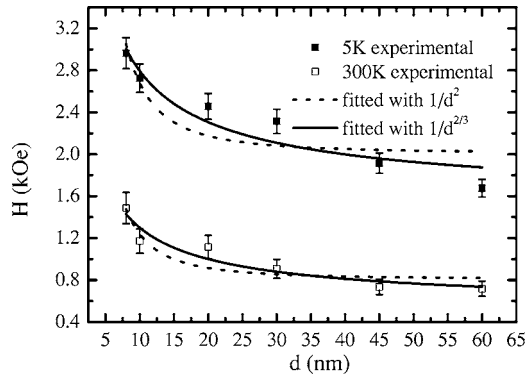

FIG. 3. Coercivity parallel to the wire axes as a function of the nanowire diameter. The solid squares are the experimental results, whereas the solid and dashed lines are the fitted results using the curling and buckling reversal modes, respectively.

The dotted line is the fitted result for the curling reversal mode. The fitted exchange parameters are $A=1.25\times10^{-12}$ A/m and $A=8.02\times10^{-13}$ A/m at 5 and 300 K, respectively, which are in agreement with the values of the magnetic materials.[29]

Since the homogeneous rotations and the curling mode represent extreme nucleation modes with vanishing exchange energy and vanishing stray fields, respectively, theoretical prediction has shown that there may exist another reversal mode, i.e., buckling reversal mode. The buckling mode can be described approximately as a homogeneous rotation for each cross section, whereas with a sinusoidal variation along the cylinder axis. For the magnetization buckling reversal mode, the dependence of coercive fields on nanowire diameter can be written as[30]

$$H_{c\|}=\frac{2\pi kA}{\mu_0 M_s}\frac{1}{d^{2/3}}+H_a. \tag{2}$$

The solid lines in Fig. 3 are the fitted curves for the buckling reversal mechanism using Eq. (2). Although the difference of fitting curves corresponding to these two modes is not so large, our simulation results for magnetization configuration near coercivity (Fig. 2) demonstrate that the reversal starts at one end of the wire and then propagates through the whole wire. The variation of the amplitude of magnetization along the cylinder axis at the two sides of nanowire implies that the buckling mode is favorable in magnetization reversal process.

In our previous work, the temperature dependence of coercivity of the Fe_3Pt nanowire arrays with the diameter $d=10$ nm has been discussed in detail.[21] It was demonstrated that in addition to the intrinsic variation of the K, A, and M_S, the thermal fluctuations play an important role in the magnetization reversal process of the nanowire arrays. If we take the thermal effect into account with the energy barrier proposed by Néel[31] and Brown,[32] which is usually written by

$$\Delta E=KV\left(1-\frac{H}{H_0}\right)^m. \tag{3}$$

The temperature dependence of the coercivity has been interpreted by the above thermally activated reversal mechanism with $m=2.0$, suggesting the nanowires exhibit similar behavior as that of the Stoner-Wohlfarth model, corresponding to the nanowires with the easy magnetization direction along the wire axes. Due to the thermally activated reversal mechanism playing an important role in the Fe_3Pt nanowire arrays, the time dependence of the magnetization $M(t)$ would show a strong magnetic viscosity effect. For the nanowire arrays, by applying an external magnetic field, the probability of the magnetization jumped over the energy barrier is $P(t)=e^{-t/\tau}$. Therefore, the magnetization is expected to vary exponentially with time $M(t)=M(0)e^{-t/\tau}$, where $\tau=\tau_0 e^{-\Delta E/k_BT}$. The exponential time dependence of magnetization has been attributed to the single energy barrier height. However, exponential behavior has seldom been observed due to different energy barriers coming from the distribution of the anisotropy and size in real systems. The grains with smaller volumes or anisotropy will decay faster and the ob-

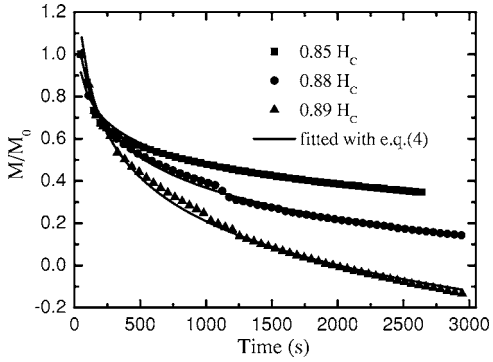

FIG. 4. Time dependence of the magnetization $M(t)$ at 300 K with different applied fields for the Fe_3Pt nanowire arrays with the wire diameter $d=10$ nm.

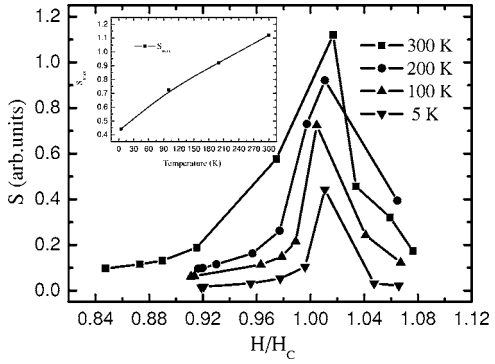

FIG. 5. Field dependence of magnetic viscosity coefficients $S(T,H)$ at different temperatures. The inset shows the maximum values of the magnetic viscosity coefficients S_{max} as a function of temperature.

served dynamics of the magnetization decay is more like the superposition of the exponential decays with different energy barriers. As a result, the observed time dependence magnetization is approximately linearly dependent on the logarithm of time as follows:

$$M(t) = M_0[1 - S(T,H)\ln t], \tag{4}$$

where $S(T,H)$ is the magnetic viscosity coefficient caused by the thermally activated magnetization reversal. The magnetic relaxation measurement procedure is as follows: the temperature is fixed at the desired value and saturated with a positive applied field, then the desired negative reversed field is set and held constant, and the magnetization decay measurements $M(t)$ have been measured for thousands of seconds.

Figure 4 illustrates the time dependence of magnetization $M(t)$ for the Fe_3Pt nanowire arrays with the wire diameter $d=10$ nm at 300 K in different fields. It appears that the magnetization has logarithmic time dependence, exhibiting a typical relaxation behavior. Since the magnetic relaxation behavior is significant around H_c, we chose the applied fields of $0.85H_c$, $0.88H_c$, and $0.89H_c$ as an example to plot in Fig. 4. According to Eq. (4), the magnetic viscosity coefficients $S(T,H)$ can be obtained by fitting the time dependence of magnetization. The small deviation in the M/M_0 observed at 1100 and 1250 s for applied fields of $0.88H_c$, and $0.89H_c$ is due to the measurement error. Figure 5 shows the field dependence of magnetic viscosity coefficients $S(T,H)$ at different temperatures for Fe_3Pt nanowire arrays, from which it can be seen that the magnetic viscosity coefficients increase with increasing temperature. The viscosity coefficients S present the peak values near the coercive fields H_c with different temperatures. The maximum values of the magnetic viscosity coefficients S_{max} are observed to increase with increasing temperature, as plotted in the inset of Fig. 5.

Bruno *et al.* have reported that single activation energy barrier fails to describe the observed relaxation phenomena with perpendicular easy magnetization. If it is assumed that there exists a certain distribution of the energy barrier, it should be[33]

$$-\frac{dM(t)}{d\ln(t)} = \frac{k_B T}{\Delta E_A}. \tag{5}$$

Therefore, $S(T,H)$ increases with increasing temperature (Fig. 5). On the other hand, the energy barrier with the Stoner-Wohlfarth model is controlled mainly by shape anisotropy, having the minimum value when the applied fields are near the coercive field, indicating the strongest magnetic viscosity effects.

Temperature dependence of the magnetic relaxation would further allow us to get insight into the understanding of the magnetic properties of nanowires and determine the parameter of the activation volume V^*, which has the meaning of the magnetization initially reversed to overcome the energy barrier during the thermally activated reversal process. The activation volume can be experimentally deduced by measuring the time dependence of the magnetization $M(t)$, which can be expressed as

$$V^* = \frac{k_B T}{M_s \left(\frac{H_2 - H_1}{\ln t_2 - \ln t_1} \right)\Big|_{M_{irr}}}. \tag{6}$$

Usually the activation volume is dependent on temperature and wire diameter. As discussed above, magnetization reversal is initiated by thermally activated reversal process with the energy barrier $\Delta E = KV_0(1-H/H_0)^2$. According to the definition of the activation volume $V^* = -(1/M_s)(\partial \Delta E/\partial H)$, activation volume can be given by

$$V^* = \frac{1}{2} V_0^{1/2} \left[\frac{k_B T \ln(f_0 \tau)}{K} \right]^{1/2}, \tag{7}$$

where K is the anisotropy constant, f_0 is the attempt frequency, and τ is the relaxation time. Due to the nonlinearity of the energy barrier, thermal activation volume V^* is usually different from the physical volume V_0.

Figure 6(a) shows the activation volume V^* as a function of temperature for the wire diameter $d=10$ nm. It can be seen that by increasing the temperature, the activation volumes V^* increase with the values from 30 to 240 nm^3. By fitting the experimental points with Eq. (7), it can be seen

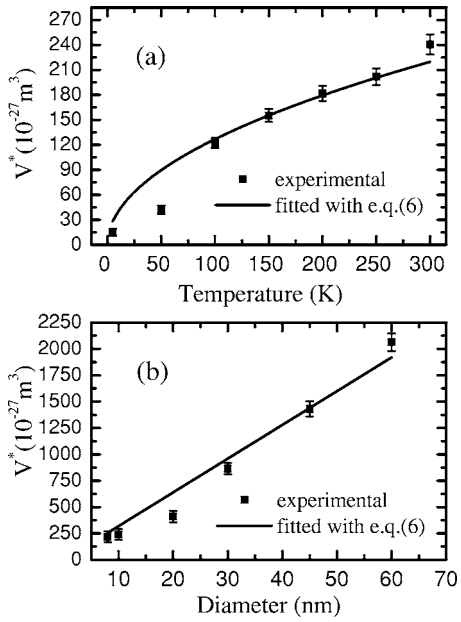

FIG. 6. (a) Activation volume V^* dependence on temperature for the wire diameter $d=10$ nm. (b) Activation volume V^* as a function of wire diameter at 300 K. The solid points are the experimental data and the solid lines are the fitting results with Eq. (7).

obviously that the activation volume V^* is roughly consistent with $T^{1/2}$ for the temperature range of 5–300 K. Assuming that the single wire volume is $V_0=\frac{1}{4}\pi d^2 L$, the activation volume V^* should be proportional to the wire diameter d. Figure 6(b) shows that the activation volume V^* increases with diameter from 200 nm^3 for $d=8$ nm up to 2000 nm^3 for $d=60$ nm. The activation volume V^* is 1 order of magnitude smaller than that of the wire volume for all the wire diameters, which confirms the localized mechanism with thermally activated reversal process.

IV. CONCLUSION

In summary, magnetization reversal mechanism and magnetic relaxation of the Fe_3Pt nanowire arrays with different diameters have been investigated by means of micromagnetic simulation and magnetization measurements. The nanowire arrays show strong magnetic viscosity effect, which is much evident at high temperatures and strongest near the coercive fields of the nanowire arrays. The activation volume dependence on temperature and diameter is consistent with the prediction of the thermally activated magnetization reversal mechanism.

ACKNOWLEDGMENTS

This work was supported by the State Key Project of Fundamental Research and the National Natural Science Foundation of China.

*Corresponding author. Electronic address: zhcheng@aphy.iphy.ac.cn

[1] P. M. Paulus, F. Luis, M. Kröll, G. Schmid, and L. J. de Jongh, J. Magn. Magn. Mater. **224**, 180 (2001).
[2] R. Skomski, J. Phys.: Condens. Matter **15**, R841 (2003).
[3] J. Mallet, K. Y. Zhang, C. L. Chien, T. S. Eagleton, and P. C. Searson, Appl. Phys. Lett. **84**, 3900 (2004).
[4] M. Zheng, L. Menon, H. Zeng, Y. Liu, S. Bandyopadhyay, R. D. Kirby, and D. J. Sellmyer, Phys. Rev. B **62**, 12282 (2000).
[5] L. Sun, P. C. Searson, and C. L. Chien, Phys. Rev. B **61**, R6463 (2000).
[6] R. Ferré, K. Ounadjela, J. M. George, L. Piraux, and S. Dubois, Phys. Rev. B **56**, 14066 (1997).
[7] H. Zeng, R. Skomski, L. Menon, Y. Liu, S. Bandyopadhyay, and D. J. Sellmyer, Phys. Rev. B **65**, 134426 (2002).
[8] R. Skomski, H. Zeng, M. Zheng, and D. J. Sellmyer, Phys. Rev. B **62**, 3900 (2000).
[9] Y. C. Sui, R. Skomski, K. D. Sorge, and D. J. Sellmyer, Appl. Phys. Lett. **84**, 1525 (2004).
[10] D. Kelly, J.-E. Wegrowe, T. Truong, X. Hoffer, and J.-P. Ansermet, Phys. Rev. B **68**, 134425 (2003).
[11] W. Wernsdorfer, K. Hasselbach, A. Benoit, B. Barbara, B. Doudin, J. Meier, J.-Ph. Ansermet, and D. Mailly, Phys. Rev. B **55**, 11552 (1997).
[12] W. Wernsdorfer, B. Doudin, D. Mailly, K. Hasselbach, A. Benoit, J. Meier, J.-Ph. Ansermet, and B. Barbara, Phys. Rev. Lett. **77**, 1873 (1996).
[13] W. Wernsdorfer, K. Hasselbach, A. Sulpice, A. Benoit, J.-E. Wegrowe, L. Thomas, B. Barbara, and D. Mailly, Phys. Rev. B **53**, 3341 (1996).
[14] W. Wernsdorfer, E. B. Orozco, K. Hasselbach, A. Benoit, B. Barbara, N. Demoncy, A. Loiseau, H. Pascard, and D. Mailly, Phys. Rev. Lett. **78**, 1791 (1997).
[15] A. Encinas-Oropesa, M. Demand, L. Piraux, I. Huynen, and U. Ebels, Phys. Rev. B **63**, 104415 (2001).
[16] U. Ebels, J. L. Duvail, P. E. Wigen, L. Piraux, L. D. Buda, and K. Ounadjela, Phys. Rev. B **64**, 144421 (2002).
[17] S. Kolesnik, B. Dabrowski, J. Mais, D. E. Brown, R. Feng, O. Chmaissem, R. Kruk, and C. W. Kimball, Phys. Rev. B **67**, 144402 (2003).
[18] C. Leighton and Ivan K. Schuller, Phys. Rev. B **63**, 174419 (2001).
[19] S. J. Collocott and J. B. Dunlop, Phys. Rev. B **66**, 224420 (2002).
[20] A. Enders, D. Repetto, D. Peterka, and K. Kern, Phys. Rev. B **72**, 054446 (2005).
[21] J. H. Gao, Q. F. Zhan, W. He, D. L. Sun, and Z. H. Cheng, Appl. Phys. Lett. **86**, 232506 (2005).
[22] The simulation code from object oriented micromagnetic framework (OOMMF) by M. Donahue and D. Porter is used, http://math.nist.gov/oommf
[23] R. Hertel, J. Appl. Phys. **90**, 5752 (2001).
[24] M. A. I. Nahid and Takao Suzuki, IEEE Trans. Magn. **39**, 2723 (2003).
[25] Q. F. Zhan, J. H. Gao, Y. Q. Liang, N. L. Di, and Z. H. Cheng,

Phys. Rev. B **72**, 024428 (2005).
[26] E. H. Frei, S. Shtrikman, and D. Treves, Phys. Rev. **106**, 446 (1957).
[27] A. Aharoni and S. Shtrikman, Phys. Rev. **109**, 1522 (1958).
[28] R. Skomski and J. M. D. Coey, *Permanent Magnetism* (Institute of Physics, Bristol, 1999).
[29] R. C. O'Handley, *Modern Magnetic Materials: Principles and Applications* (Wiley, New York, 2000).
[30] F. C. Pu, Y. J. Wang, and C. H. Shang, *Aspects of Modern Magnetism* (World Scientific, Singapore, 1995).
[31] L. Neel, Ann. Geofis. **5**, 99 (1949).
[32] W. F. Brown, Jr., Phys. Rev. **130**, 1677 (1963).
[33] P. Bruno, G. Bayreuther, P. Beauvillain, C. Chappert, G. Lugert, D. Renard, J. P. Renard, and J. Seiden, J. Appl. Phys. **68**, 5759 (1990).